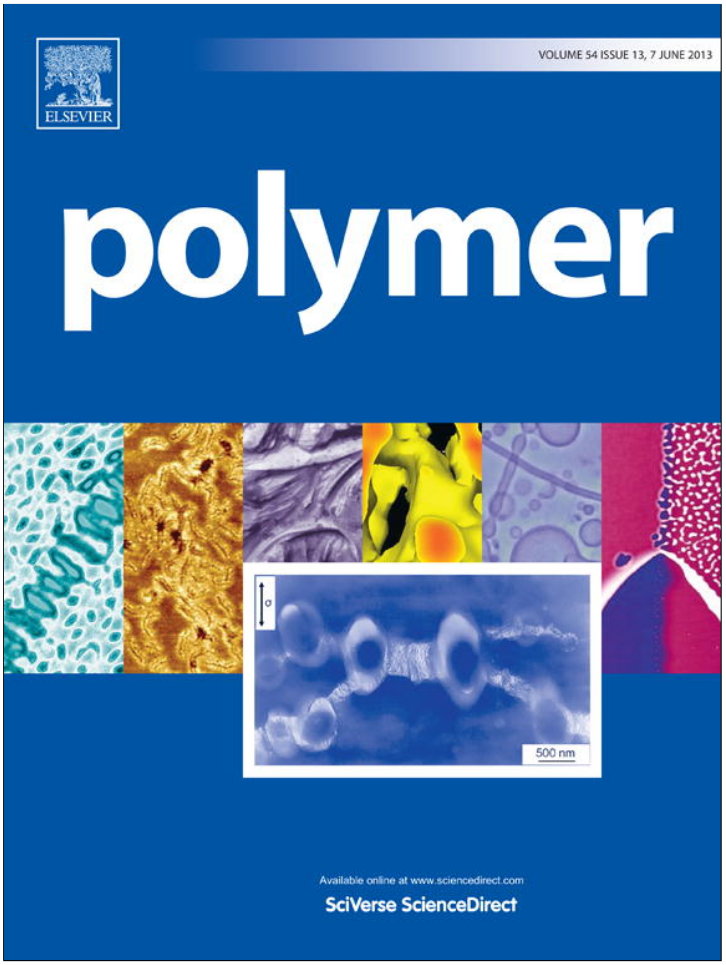
Provided for non-commercial research and education use.
Not for reproduction, distribution or commercial use.



This article appeared in a journal published by Elsevier. The attached copy is furnished to the author for internal non-commercial research and education use, including for instruction at the authors institution and sharing with colleagues.

Other uses, including reproduction and distribution, or selling or licensing copies, or posting to personal, institutional or third party websites are prohibited.

In most cases authors are permitted to post their version of the article (e.g. in Word or Tex form) to their personal website or institutional repository. Authors requiring further information regarding Elsevier's archiving and manuscript policies are encouraged to visit:

http://www.elsevier.com/authorsrights

Author's personal copy

Polymer 54 (2013) 3314–3323

Contents lists available at SciVerse ScienceDirect

Polymer

journal homepage: www.elsevier.com/locate/polymer

Vulcanization kinetics of graphene/natural rubber nanocomposites

Jinrong Wu, Wang Xing, Guangsu Huang*, Hui Li, Maozhu Tang, Siduo Wu, Yufeng Liu

College of Polymer Science and Engineering, State Key Laboratory of Polymer Materials Engineering, Sichuan University, Chengdu 610065, China

ARTICLE INFO

Article history:
Received 18 February 2013
Received in revised form
3 April 2013
Accepted 17 April 2013
Available online 25 April 2013

Keywords:
Graphene
Rubber
Vulcanization kinetics

ABSTRACT

In the present work, the influence of graphene (GE) on the vulcanization kinetics of natural rubber (NR) with sulfur curing system was investigated in detail for the first time. It is found that on adding graphene the induction period of the vulcanization process is remarkably depressed, whereas the vulcanization rate is enhanced at low graphene loading and then suppressed. As a result, the optimum cure time decreases dramatically at first and subsequently shows a slight increase with increasing graphene loading. At the same time, the crosslinking density of NR increases monotonically, because graphene takes part in the vulcanization process. The exothermal peak of the vulcanization reactions is split into two peaks on adding $\geq$0.5 phr graphene. It is interpreted in terms of two reaction stages, i.e., chemical reaction controlling stage and diffusion controlling stage. The activation energy of the former stage decreases with increasing graphene loading, while that of the latter stage is higher than the former one and increases with graphene loading. A possible mechanism was proposed to interpret the accelerating effect of graphene and the enhanced crosslinking density of NR.

© 2013 Elsevier Ltd. All rights reserved.

1. Introduction

It is well-known that the mechanical properties of rubbers strongly depend on the vulcanization state. Thus the vulcanization reactions and kinetics of unfilled rubbers had been intensively investigated and well established decades of years ago [1]. However, with the rapid development in nanocomposites, some recent studies have shown that the vulcanization kinetics of rubbers could be changed significantly by incorporation of nanofillers. López-Manchado and coworkers [2] were the first to explore the influence of unmodified clay and organoclay on the vulcanization kinetics of natural rubber (NR). It was found that octadecylamine modified clay behaved as an accelerator for NR vulcanized with sulfur, but unmodified clay had little effect on the vulcanization process. The accelerating effect of organoclay was attributed to the surface modifier (i.e., octadecylamine) that could accelerate the vulcanization process. Several subsequent works on different rubber matrices leaded to the same conclusion [3–7]. Nevertheless, some other works observed an opposite phenomenon, i.e., organoclays could retard the vulcanization process. Lakshminarayanan et al. [8] found that di(hydrogenated tallow-alkyl) dimethyl ammonium modified organoclays could delay the peroxide vulcanization process of fluoroelastomer, which was attributed to the scavenging of free radicals by organoclays. Sepehri et al. [9] found that the formation of organoclay network could limit the diffusion and accessibility of curing agents to the vulcanization sites, thus retarded the vulcanization of butyl rubber with sulfur. Carbon nanotubes (CNTs) also have significant influence on the vulcanization process of rubbers. López-Manchado et al. [10] showed that single-walled carbon nanotubes (SWCNTs) reduced the activation energy and accelerated the crosslinking reaction of NR with sulfur. Nevertheless, they did not interpret the mechanism of the accelerating effect of SWCNTs. Sui et al. [11] found that the scorch time of NR vulcanized with sulfur decreased with the addition of acid-treated CNTs, but the optimum cure time was barely affected. On the contrary, Shanmugharaj et al. [12] and Faclo et al. [13] demonstrated that the presence of certain functional groups such as carboxylic acid groups and quinone oxygen atoms could absorb the basic accelerator species, thus delayed the vulcanization process of NR. In summary, the above mentioned works suggest that the vulcanization kinetics in the rubber based nanocomposites is complicated, and some works even lead to controversial conclusions. More complicated are different nanofillers having different influence on the vulcanization kinetics. For example, some other nanofillers (e.g. halloysite nanotube, zinc dimethacrylate and zinc oxide) were also reported to have complicated influence on the vulcanization kinetics of rubbers [14–16].

In recent years, graphene (GE) has attracted tremendous attention in polymer nanocomposites. Many works have been done to

* Corresponding authors. Tel./fax: +86 28 85463433.
E-mail addresses: wujinrong@scu.edu.cn (J. Wu), guangsu-huang@hotmail.com (G. Huang).

0032-3861/$ – see front matter © 2013 Elsevier Ltd. All rights reserved.
http://dx.doi.org/10.1016/j.polymer.2013.04.044

Author's personal copy

improve the mechanical properties, electrical conductivity, gas permeability and thermal stability of thermoplastic polymers [17–22]. However, there are only a few works that incorporate graphene into elastomers [23–31]. Prud'Homme et al. [23] firstly added thermally-reduced graphene into several elastomers, including NR, styrene butadiene rubber (SBR) and poly(dimethyl siloxane). Their work demonstrated the prominent potential of graphene in improving the mechanical and gas barrier properties of elastomers. Subsequently, Zhan et al. [24,25] and Potts et al. [26] blended chemically reduced graphene with NR via latex compounding during which graphene was stabilized by ultrasonic field or potassium hydroxide, and the processing–morphology–property relationships of resulting nanocomposites were studied in detail. However, the influence of graphene on the vulcanization kinetics of rubbers, which is of primary importance to prepare graphene/rubber nanocomposites, has not been well studied. Only few works reported the accelerating effect of graphene, while the details of the vulcanization kinetics and the underlying mechanism were not investigated [28,29]. Our previous work observed that bis(triethoxysilylpropyl)tetrasulfide modified graphene oxide accelerated the vulcanization process of NR with dicumyl peroxide [28]. Hernández et al. [29] mentioned that thermally-reduced graphene promoted the vulcanization process of NR with sulfur, but the graphene loading in their nanocomposites was only up to 1 phr, and it is of interest to investigate the vulcanization kinetics of nanocomposites with higher filler loading.

In the present work, a new latex mixing method without having to stabilize graphene using additional surfactant or ultrasonic field developed in a previous work was used to prepare GE/NR nanocomposites [51]. In the method, aqueous dispersion of GO was mixed with NR latex, and the mixture was co-coagulated with saturated solution of sodium chloride to form a suspension of micro-sized particles, in which GO was isolated by the nanospheres of NR latex to achieve molecular level dispersion. Subsequently, hydrazine hydrate was added to reduce GO in situ. The vulcanization kinetics of the resulting GE/NR nanocomposites was studied in detail.

2. Experimental

2.1. Chemicals

Highly-purified graphite flakes (99.99%) were purchased from Qingdao Ruisheng Graphite Company, China. NR latex (60 wt% of NR content) was obtained from the Chinese Academy of Tropical Sciences. Curing reagents including sulfur, zinc oxide (ZnO), N-cyclohexyl-2-benzothiazolesulfenamide (CZ), stearic acid (SA), and antioxidant N-isopropyl-N′-phenyl-p-phenylene diamine (4010NA) are all kindly provided by Sichuan Haida Rubber Group Co., Ltd. Other reagents were all of analytical-grade and commercially available.

2.2. Preparation of graphite oxide

Graphite oxide was synthesized by Hummers' method from graphite flakes [32], and then dispersed in water by ultrasonic-treatment. The suspension was centrifugated at 10,000 r.p.m for 10 min to remove any unexfoliated graphite, thus fully exfoliated GO suspension was obtained and subsequently placed in a vacuum oven at 70 °C for several days to remove the water.

2.3. Preparation of GE/NR nanocomposites

Graphite oxide was re-dispersed in water to obtain aqueous GO suspension at a concentration of 1 mg/mL by bath sonication. Natural rubber latex was diluted to a solid fraction of 20%, and then mixed with different amounts of aqueous GO suspension by mechanical stirring to produce nanocomposites with different GE loading. After 30 min of stirring, the homogeneous mixture was co-coagulated with saturated NaCl solution to form a particles' suspension. Hydrazine hydrate was added to the suspension with a ratio of 30 μL per 1 mg of GO, which was allowed to stir for 24 h at 100 °C to reduce GO in situ. The solids were filtrated and washed with deionized water and then vacuum dried in an oven at 60 °C for 48 h. For comparison, a sample of unfilled NR was prepared from natural rubber latex subjecting to the same procedures that were used to prepare GE/NR nanocomposites. The curing agents were added in an open twin-roll mill (SK-160B, Shanghai Huaxiong Machinery Co., Ltd., China) at room temperature with a friction ratio of 1:1.2 and nip gap of ~ 1 mm. The curing formula for unfilled NR and GE/NR nanocomposites is as following: NR 100 phr, sulfur 2 phr, ZnO 5 phr, CZ 0.9 phr, steric acid 1 phr, and 4010NA 1 phr.

For comparison, curing systems with and without graphene were also prepared. 0.2 g of sulfur, 0.5 g of ZnO, 0.09 g of CZ and 0.1 g of steric acid were ground in a mortar to form a mixture of curing system without graphene. To prepare curing system with graphene, 0.1 g of dried graphene prepared by reduction of graphene oxide in aqueous suspension was added to the former system and further ground to form a homogeneous mixture.

2.4. Characterization

Wide angle X-ray diffraction (WAXD) was performed on Philips X'Pert Graphics & Identify with Ni-filtered CuKa radiation ($k = 0.154$ nm) at a generator voltage of 35 kV and generator current of 25 mA. Scanning was at a speed of 2.4°/min^{-1}, from 2° to 35°.

The dispersion state of graphene within the NR matrix was observed by a transmission electron microscope (TEM, FEI Tecnai G2 F20 S-TWIN) at an accelerating voltage of 200 kV. Ultra-thin sections were prepared using a Leica Ultracut UCT ultramicrotome with a diamond knife at −100 °C.

Raman spectra were recorded from 100 to 4000 cm^{-1} on a LABRAM HR800 confocal micro-Raman spectrometer using a 532 nm ND: YAG laser.

The vulcanization process was analyzed with a curemeter produced by Beijing Youshen Electronic Apparatus Factory (Beijing, China) at 143 °C, which is considered to be a suitable vulcanizing temperature for NR [6,52,53] Measurements of differential scanning calorimeter (DSC) at different heating rates (2, 5, 10, 15, and 20 °C/min) were performed on Q200, TA instruments. The weights of the samples were in the range of 5–7 mg.

The equilibrium swelling measurement was performed at room temperature in toluene for 7 days. After equilibrium swelling, the solvent was gently wiped off the sample surface with filter paper, w_2 was determined by deducting the weight of graphene from the overall weight of swollen sample. After drying the swollen sample at 80 °C until a constant weight was achieved, w_1 was determined by deducting the weight of graphene from the overall weight of deswollen sample.

X-ray Photoelectron Spectroscopy (XPS) measurements were performed on an XSAM800 (Kratos, Britain) using a nochromatic Mg Ka X-ray source radiation ($hv = 253.6$ eV) operated at 12 kV and 15 mA. The pressure in the analysis chamber was 2×10^{-7} Pa. The measured spectra were calibrated to binding energies for $Cu^2P_{3/2}$, $Ag^3d_{5/2}$ and $Au^4f_{7/2}$ levels. Charge effects were compensated assuming carbon $C1_s$ peak at 284.8 eV position.

3. Results and discussion

3.1. Microstructure of GE/NR nanocomposites

To characterize the dispersion state of graphene in the NR matrix, TEM and WAXD measurements were performed for the GE/NR

Author's personal copy

nanocomposites. The TEM image of the GE/NR nanocomposite with 1 phr of graphene loading is displayed in Fig. 1. It is evident that the graphene nanosheets are exfoliated into single or a-few-stacked layers, which are finely dispersed throughout the NR matrix, indicating that the latex mixing method used in the present work is efficient in dispersing graphene in the polymer matrix. The WAXD patterns of graphite oxide, graphene prepared by chemical reduction in aqueous suspension and GE/NR nanocomposites are shown in Fig. 2. It can be seen that graphite oxide shows a sharp characteristic peak at $2\theta = 11.0°$, while after reduction in aqueous suspension the peak disappears, and the resulting graphene has a broad characteristic peak centered at $2\theta = 24.7°$ due to the restack of graphene layers. The GE/NR nanocomposites display a broad amorphous peak centered at $2\theta = 18.7°$, which is attributed to the scattering of the amorphous NR matrix. Besides, there are some sharp diffraction peaks above 30°, which are assigned to the characteristic peaks of ZnO and stearic acid in the curing formula [33,34]. Except these peaks, there are no detectable characteristic peaks of graphene stacks or graphite oxide in the nanocomposites. Therefore, it can be concluded that there is no significant layer-by-layer restack of graphene in the NR matrix, even when the graphene loading is up to 5 phr.

In order to evaluate the reduction of graphite oxide into graphene, Raman spectroscopy is performed. As shown in Fig. 3, the first order Raman spectrum of graphite oxide contains a G band at 1588 cm^{-1} and a D band at 1347 cm^{-1}. The G band and D band are assigned to the in-phase vibration of the graphite lattice and the structural defects, respectively. After reduction, the intensity ratio of D band to G band (I_D/I_G) increases from 0.89 for graphite oxide to 1.38 for graphene. The increase of I_D/I_G after reduction has been observed by many other works [35–39]. Stankovich et al. [35] attributed the increase of I_D/I_G in the chemically reduced graphene to the smaller size of numerous newly-formed graphitic domains. Paredes et al. [39] found that the carbon lattice in the chemically reduced graphene was essentially graphitic, but highly defected. The I_D/I_G value is 1.37 in the GE/NR nanocomposite with 5 phr of graphene loading, which is basically equal to that of graphene prepared by chemical reduction in aqueous suspension, suggesting that GO is effectively reduced in the GE/NR nanocomposites. XPS measurement was also conducted to further confirm the effective reduction of GO, as shown in Fig. 4. The $C1_s$ spectrum of GO suggests that there are significant amounts of oxygen functionalities, including C–O, C=O and O–C=O. A multi-Gaussian-peak fitting indicates that the nonoxygenated carbon only contributes 54.7% to the area under the $C1_s$ peak. After reduction, its contribution is 75.4% to the total area, which is consistent with the result of other works [25,35,38]. Moreover, reacting with hydrazine hydrate introduces an additional peak at 286 eV corresponding to carbon bounded to nitrogen [35]. These results confirm the effective reduction of GO. Besides, the $C1_s$ spectrum of graphene still shows the same oxygen functionalities as that of GO. Although their peak intensities are greatly suppressed, they still contributes 20.9% to the total area. These oxygen functionalities as mentioned later will have strong influence on the vulcanization kinetics of NR.

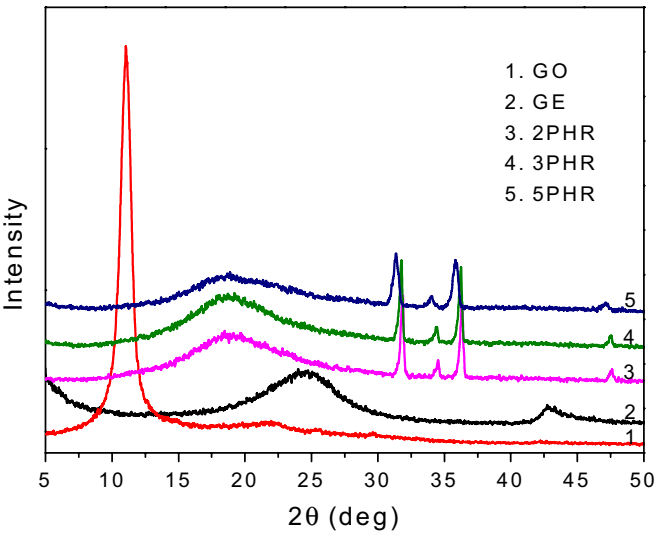


Fig. 2. XRD patterns of graphite oxide, graphene prepared by chemical reduction in aqueous suspension and GE/NR nanocomposites with graphene loadings of 2 phr, 3 phr and 5 phr.

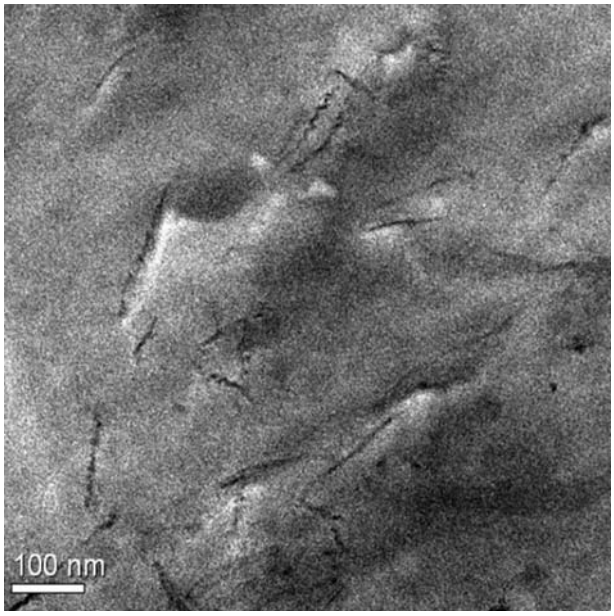


Fig. 1. TEM images of the GE/NR nanocomposite with 1 phr of graphene loading.

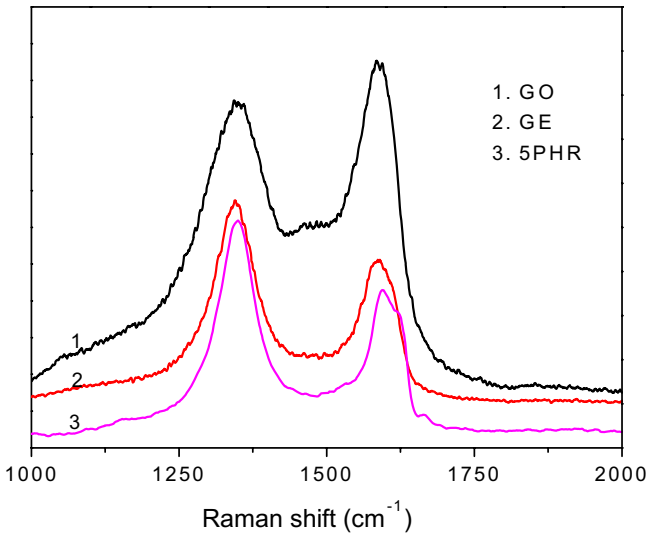


Fig. 3. Raman spectra of graphite oxide, graphene prepared by chemical reduction in aqueous suspension and the GE/NR nanocomposite with 5 phr of graphene loading.

Author's personal copy

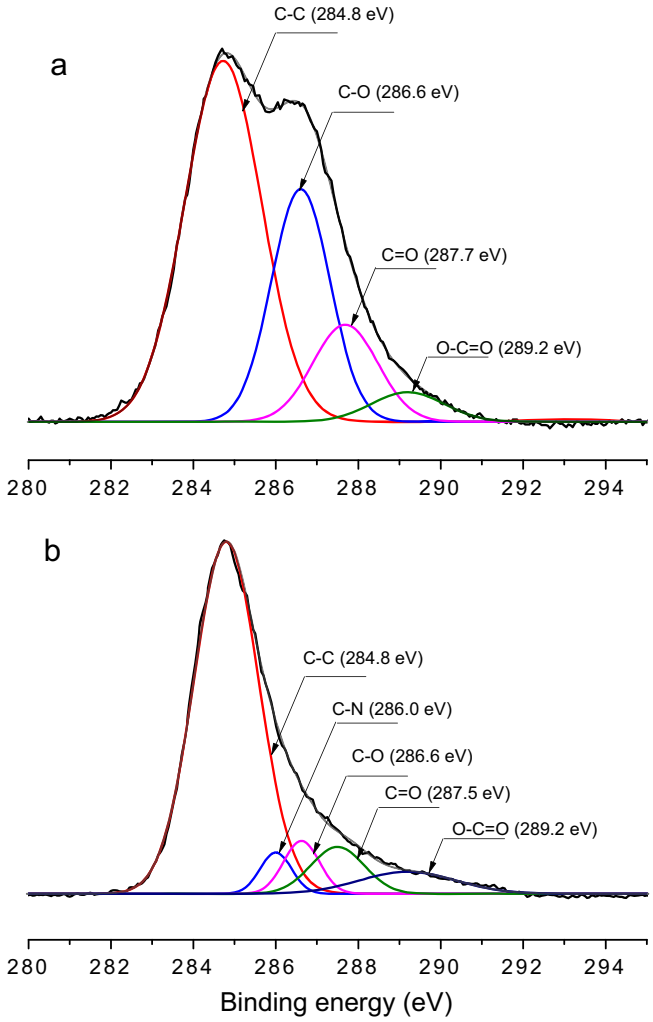


Fig. 4. $C1_s$ XPS spectra of GO (a) and graphene (b).

3.2. Vulcanization kinetics of GE/NR nanocomposites studied by curemeter

To illustrate the influence of graphene loading on the vulcanization kinetics of NR, the curing curves of unfilled NR and GE/NR nanocomposites are shown in Fig. 5. It is clear that the curing curves are systematically shifted toward the short time side with increasing graphene loading, suggesting that the vulcanization process of NR is noticeably accelerated. At the same time, the presence of graphene increases both the minimum and maximum torque values of the curing curves. To get more specific information, some important vulcanization parameters, including t_{10} cure time (which can also be used to measure scorch safety), t_{90} cure time (i.e., optimum cure time), the difference between t_{10} cure time and t_{90} cure time ($t_{90}-t_{10}$), and the difference between minimum and maximum torque (ΔS) are determined from the curing curves, as shown in Fig. 6.

The t_{10} cure time is the time to increase the torque 10% above the minimum torque. It can be used to characterize the induction period, during which the active accelerator complex is formed via reaction of the accelerator and the activator, and subsequently the complex reacts with molecular sulfur to form a distribution of polysulfide species [1,40,41]. It is clear in Fig. 6(a) that t_{10} decreases rapidly when the graphene loading is lower than 1 phr, and then shows a gentle decrease. It suggests that the presence of a small

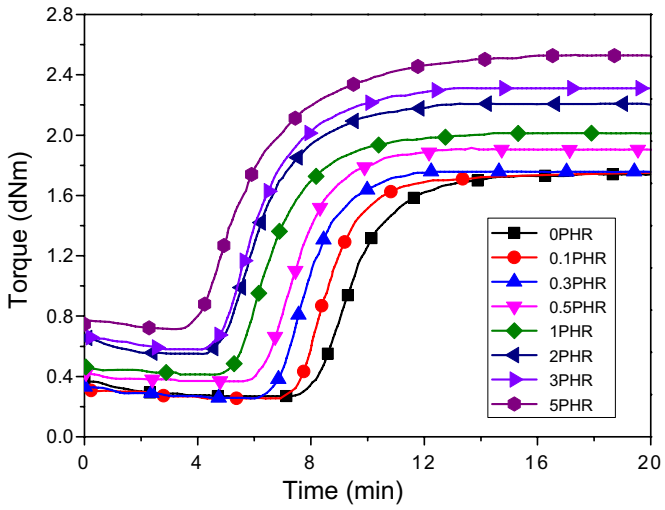


Fig. 5. Curing curves of NR and GE/NR nanocomposites with different graphene loadings.

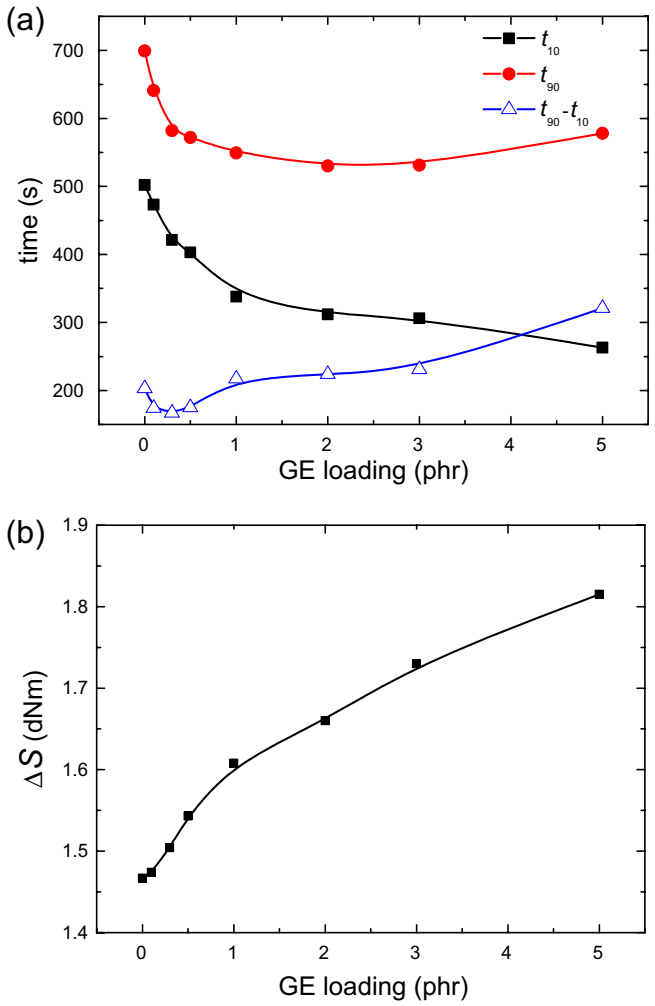


Fig. 6. Effect of graphene loading on the vulcanization parameters determined from the curing curves. (a) Scorch time, optimum cure time and the difference between scorch time and optimum time; (b) the difference between minimum and maximum torque (ΔS). The lines are the guides to the eyes.

Author's personal copy

amount of graphene greatly reduces the induction period of the vulcanization process. The optimum cure time, t_{90}, is the time to increase the torque 90% above the minimum torque. During this process, the activated polysulfide species react with the unsaturated sites on the rubber chains to form crosslink precursors, which are accelerator-terminated polysulfidic pendant groups attached to the rubber chains. These crosslink precursors subsequently react with additional unsaturated sites or other crosslink precursors resulting in polysulfidic crosslinks [1,40,41]. Similar to the case of t_{10}, t_{90} is also strongly reduced when the graphene loadding is lower than 1 phr, as shown in Fig. 6(a). Thus, incorporating a small amount of graphene remarkably accelerates the crosslinking reactions. However, too much graphene loading (exceeding 3 phr) inversely raises t_{90}, although t_{10} is still decreasing. As a result, $t_{90}-t_{10}$ decreases at first, but then inversely increases. Actually, $t_{90}-t_{10}$ can be used to evaluate the vulcanization rate, where higher vulcanization rate leads to smaller $t_{90}-t_{10}$. It can be inferred from Fig. 6(a) that the vulcanization rate is promoted at low graphene loading (<1 phr), whereas it is suppressed subsequently. Therefore, the vulcanization rate of the GE/NR nanocomposites with the graphene loading higher than 1 phr is even slower than that of unfilled NR, although the overall cure time is reduced due to shorter induction period.

The difference between minimum and maximum torque, ΔS, is generally assumed to be proportional to the crosslinking density [2]. Thus it can be deduced from Fig. 6(b) that the crosslinking density of the GE/NR nanocomposites increases with increasing graphene loading. The conclusion can be confirmed by the equilibrium swelling measurements in toluene, as shown in Fig. 7. It can be found that the equilibrium swelling ratio (which is defined as w_2/w_1, w_1 is the weight of rubber in the deswollen rubber and w_2 is the weight of rubber and solvent in the swollen sample) decreases with increasing graphene loading, indicating that the addition of graphene raises the crosslinking density of NR. On the basis of the Flory–Rehner equation, the crosslinking density was determined [42]:

$$-\left[\ln(1-v_r)+v_r+\chi v_r^2\right] = V_0 n\left(v_r^{1/3}-v_r/2\right) \tag{1}$$

where v_r is the volume fraction of the rubber in the swollen mass, V_0 is the molar volume of the solvent (106.2 cm^3 for toluene), n is the number of active network chain segments per unit of volume (crosslinking density), and χ is the Flory–Huggins polymer–solvent interaction term. The value of χ for NR in toluene is 0.393 [43]. The value of v_r is attained according to:

$$v_r = \frac{w_2/\rho_2}{w_2/\rho_2+(w_1-w_2)/\rho_1} \tag{2}$$

where ρ_1 and ρ_2 are the densities of the solvent and the rubber, respectively. Calculated by Eq. 1, the crosslinking densities of unfilled NR and GE/NR nanocomposites are also presented in Fig. 7. It can be seen that the crosslinking density of unfilled NR is 1.27×10^{-4} mol/cm^3, and it increases monotonically with the addition of graphene. An almost two folds increase in crosslinking density can be observed when the graphene loading is up to 5 phr.

Like many classical chemical reactions, the vulcanization kinetics can be modeled by a differential equation related to time and temperature, regardless of the reaction mechanism [2,7]. The equation can be written as follows:

$$d\alpha/dt = K(T)f(\alpha) \tag{3}$$

where α is the conversion, $d\alpha/dt$ is the vulcanization rate, t is the time, K is a kinetic constant at temperature T, and $f(\alpha)$ is a function corresponding to the phenomenological model.

When a curemeter is used to study the vulcanization kinetics, α is defined as follows [44]:

$$\alpha = \frac{M_t - M_0}{M_\infty - M_0} \tag{4}$$

where M_0, M, and M_∞ are the torque values at time zero, at a given curing time and at the end of the vulcanization process, respectively.

It has been generally realized that the vulcanization process is an autocatalytic reaction, thus $f(\alpha)$ is given as [2,7,15]:

$$f(\alpha) = a^m(1-\alpha)^n \tag{5}$$

where $0 \le m \le 1$ and $n \ge 1$ are both the orders of reaction.

Thus, Eq. (3) can be given as:

$$d\alpha/dt = K(T)\alpha^m(1-\alpha)^n \tag{6}$$

As shown in Fig. 8, the experimental data can be well fitted with Eq. (6). The agreement of the fitting result with the experimental data and the fractioned values of n and m indicate that the vulcanization process cannot be represented by a simple elemental reaction, but rather by various reactions which can occur

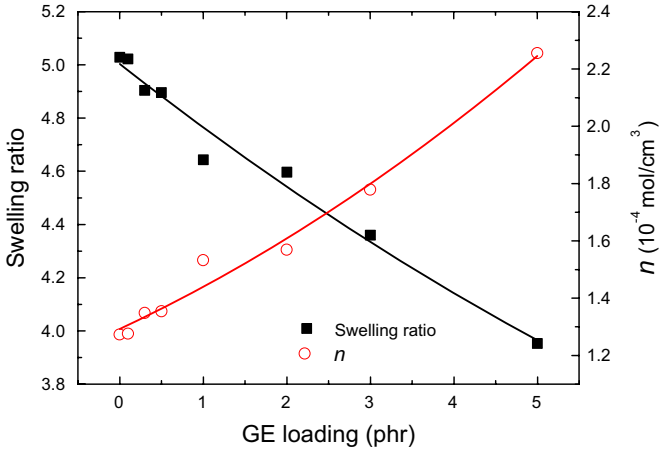


Fig. 7. The effect of graphene loading on the equilibrium swelling ratio and crosslinking density of unfilled NR and GE/NR nanocomposites. The lines are the guides to the eyes.

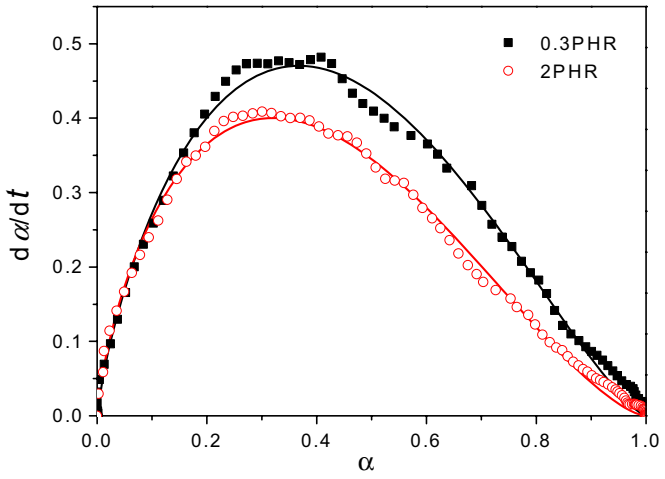


Fig. 8. Representative plotting of the derivative of α as a function of α for the GE/NR nanocomposites at 143 °C. The lines are the results predicted from Eq. (6).

Author's personal copy

simultaneously or in series, and these reactions undergo an autocatalytic process during vulcanization. The fitting parameters are listed in Table 1. It can be seen that with incorporation of graphene K increases at first and then decreases, which is consistent with the observation in Fig. 6(a) that the vulcanization rate is promoted at low graphene loading, and subsequently it is suppressed. The n values are higher than the m values, which points out the dependency of the vulcanization reaction on the initial reactants of the compound, if compared to the catalytic effect of the reaction products. $m + n$ mainly shows an increasing trend by adding graphene, which indicates that the reaction order is slightly changed when graphene takes part in the curing reaction of NR.

3.3. Vulcanization kinetics of GE/NR nanocomposites studied by DSC

DSC is another widely used technique to study the vulcanization kinetics, through monitoring the change in heat flow upon crosslinking. The representative heat flow curves of unfilled NR and GE/NR nanocomposites subjected to a heating process are shown in Fig. 9. It is interesting to note that the exothermal peak of the cure reaction splits into two peaks when the graphene loading is higher than 0.5 phr. At the same time, the intensity of the second peak becomes increasingly stronger with the dissipation of the first peak. For quantitative discussion, three characteristic temperatures of the vulcanization process, including onset temperature (T_{on}), peak temperature of the first peak (T_{p1}) and that of second peak (T_{p2}), are determined as displayed in the lower inset of Fig. 9. The results are shown in Fig. 10. It is evident that T_{on} deceases with increasing graphene loading, which well coincides with the result of curemeter that shows reduced induction period. Meanwhile, T_{p1} shifts to lower temperature, but T_{p2} shifts to higher temperature with the addition of graphene.

The mechanism leading to the appearance of the two exothermal peaks is still unknown. Since this phenomenon is not observed in the GE/NR nanocomposites with low graphene loading, certain physical factor related to the graphene loading may be the reason. Two other phenomena can be used to confirm this supposition. First, the double-peak structure is affected by heating rate, i.e., when the heating rate is low, the second peak tends to overlap with the first one. Second, isothermal heat flow curves during the vulcanization process of GE/NR nanocomposites (not shown here) do not have such a double-peak structure. Following the interpretation of Sepehri et al. [9], we consider that the diffusion of the curing agents may play an important role here. When the rubber with curing formula is subjected to a heating process, the accelerator, activator and sulfur diffuse in the rubber matrix to find each other and react with each other to form polysulfide species, which then further diffuse to contact and react with the unsaturated double bounds to form crosslinking points. In the absence of graphene or when the graphene loading is lower than 0.3 phr, the curing agents diffuse freely. Thus the vulcanization reaction proceeds smoothly without being divided into two stages. On the contrary, in the GE/NR nanocomposites with higher graphene loading, the curing agents nearby could also diffuse freely to implement the vulcanization process, thus this process is controlled by the chemical reactions. However, the curing agents isolated by graphene nanosheets need to go through tortuous paths to form polysulfide species and crosslinking points. Thus, the vulcanization process can be divided into two stages, i.e., chemical reaction controlling stage and diffusion controlling stage, corresponding to the first and second exothermal peaks, respectively.

Table 1
Kinetic parameters obtained by fitting the experimental data in Fig. 8 with Eq. (6).

GE loading (phr)	K	m	n	$m + n$
0	1.65	0.79	1.39	2.18
0.1	1.93	0.73	1.44	2.17
0.3	1.97	0.80	1.38	2.18
0.5	1.89	0.81	1.43	2.24
1	1.79	0.73	1.62	2.35
2	1.67	0.73	1.54	2.27
3	1.69	0.73	1.62	2.35
5	1.59	0.71	1.88	2.59

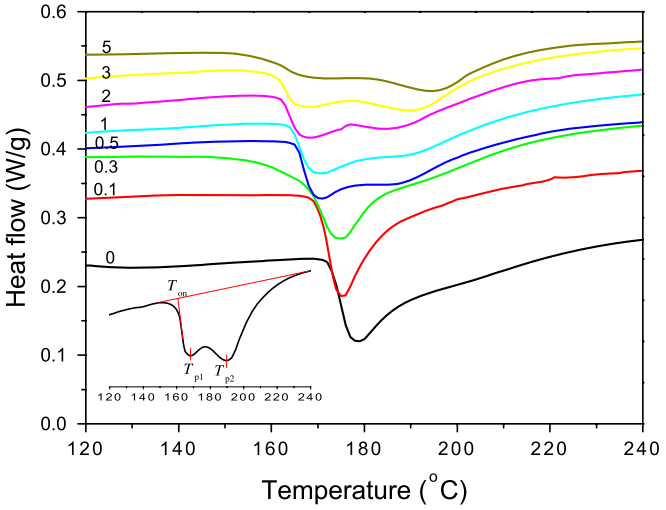


Fig. 9. Heat flow curves of NR and GE/NR nanocomposites at a heating rate of 10 °C/min. The numbers in the figure indicate the graphene loadings in the nanocomposites. The cures are shifted vertically for clarity. The lower inset shows how to determine T_{on}, T_{p1} and T_{p2}.

Fig. 11 shows the typical DSC curves recorded for the GE/NR nanocomposite with 3 phr of graphene loading at different heating rates. As the heating rate is increased, the two exothermal peaks become more and more separated. At the same time, T_{p1} and T_{p2} are both shifted toward higher temperature. The activation energy (E_a) of the vulcanization reaction can be determined from the non-isothermal cure reactions with different heat rates, while avoiding the use of any specific model. Frequently, the Ozawa method [45] and the Kissinger method [46] are used to calculate E_a with the following equations:

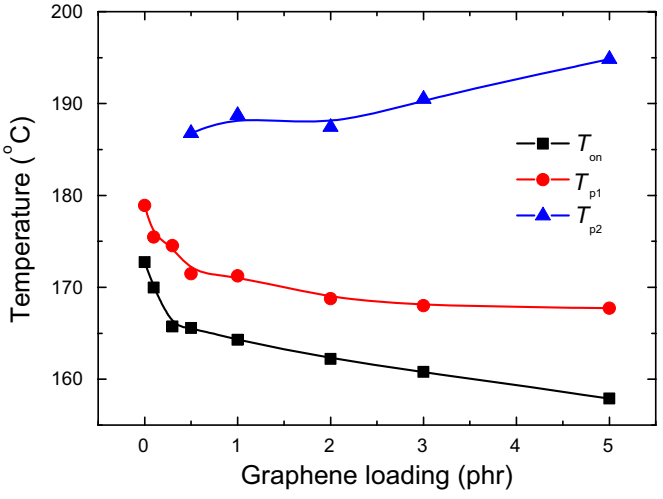


Fig. 10. Effect of graphene loading on T_{on}, T_{p1} and T_{p2}. The lines are the guides to the eye.

Author's personal copy

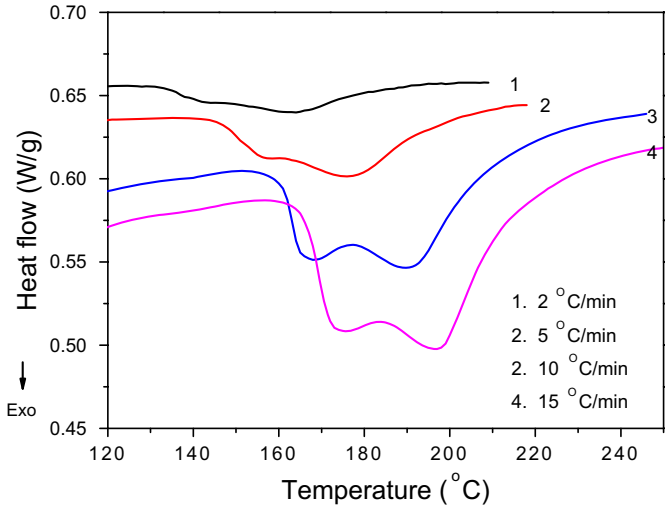


Fig. 11. Typical DSC curves recorded for the GE/NR nanocomposite with 3 phr of graphene loading at different heating rates. The curves are shifted vertically for clarity.

Table 2
The activation energy of the vulcanization reaction of the GE/NR nanocomposites.

GE loading (pHR)	E_a (kJ/mol)			
	Ozawa		Kissinger	
	T_{p1}	T_{p2}	T_{p1}	T_{p2}
0	108.8	–	101.4	–
0.1	97.6	–	90.3	–
0.3	93.5	–	86.1	–
0.5	92.9	–	85.6	–
1	95.2	–	87.9	–
2	91.7	100.9	84.5	93.5
3	90.8	101.0	83.6	93.5
5	85.7	102.6	78.6	95.2

$$\text{Ozawa method}: \quad E_a = -R\frac{d\ln\beta}{d(1/T_p)} \tag{7}$$

$$\text{Kissinger method}: \quad E_a = -R\frac{d\ln\left(\beta/T_p^2\right)}{d(1/T_p)} \tag{8}$$

where β is the heating rate, T_p is the peak temperature of the exothermal peak, and R is the gas constant. According to Eqs. (7) and (8), the plots of ln β versus $1000/T_p$ and $\ln(\beta/T_p^2)$ versus $1000/T_p$ are shown in Fig. 12(a) and (b), respectively, in which T_{p2} of the nanocomposites with 0.5 phr and 1 phr of graphene loadings is not shown due to the significant overlapping of the two exothermal peaks at low heating rates. By fitting these plots with linear functions, we can calculate E_a from the slopes of these plots. The results are shown in Table 2. Both the Ozawa method and the Kissinger method indicate that E_a of the first peak decreases with increasing graphene loading, indicating that the presence of graphene favors the chemical reaction controlling stage of the vulcanization. However, E_a of the second peak is higher than that of the first peak and shows a slight enhancement with increasing graphene loading, suggesting that the diffusion controlling stage has higher activation energy than the chemical reaction controlling stage. This is easy to understand, because in the second stage the curing agents have to overcome the energy barrier of tortuous diffusion at first and then undergo curing reaction, and the higher graphene loading makes the diffusion more difficult, which results in higher E_a value.

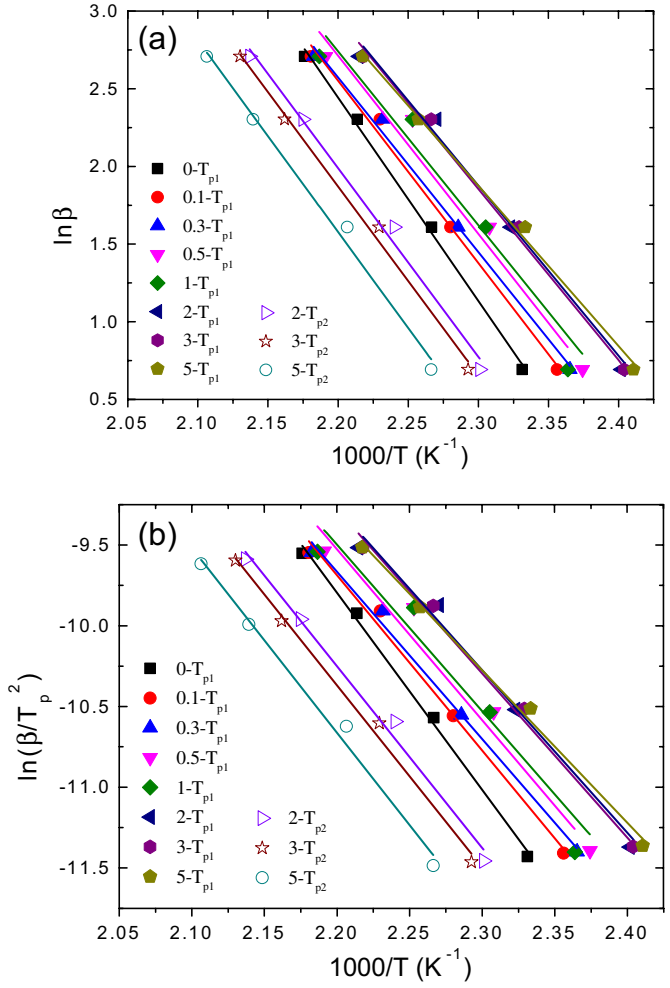


Fig. 12. Dynamic DSC for calculating E_a by (a) the Ozawa equation and (b) the Kissinger equation.

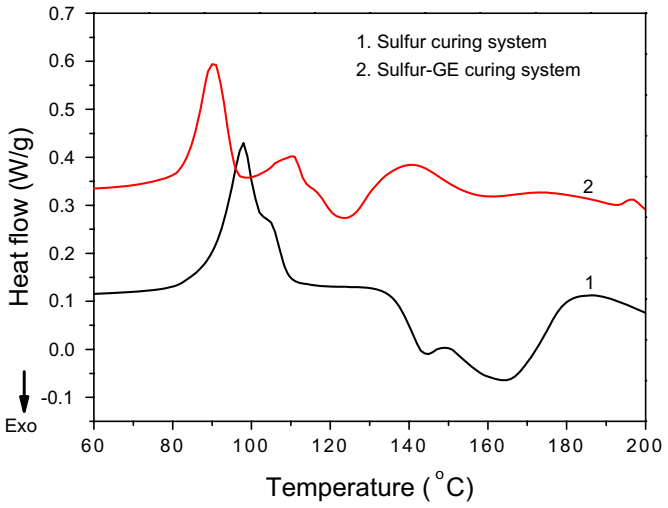
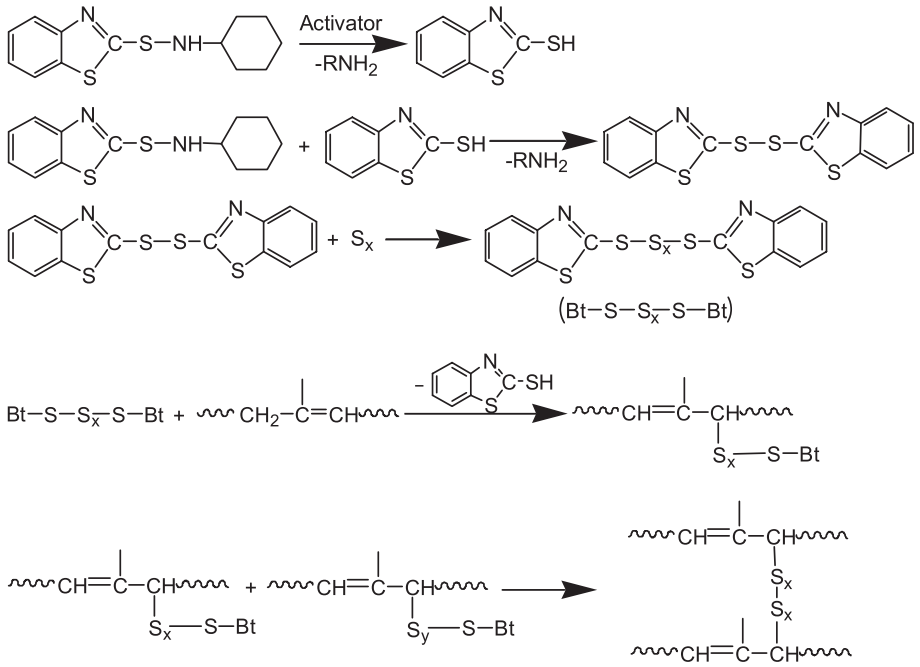


Fig. 13. The heat flow curves of sulfur curing system and sulfur-GE curing system at a heating rate of 10 °C/min. The cures are shifted vertically for clarity.

Author's personal copy

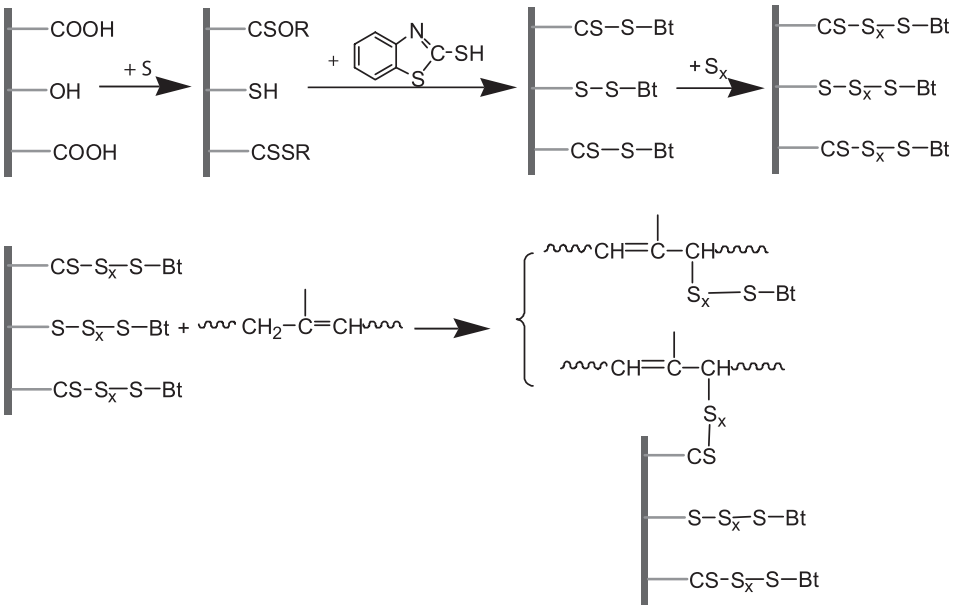


Scheme 1. Reaction scheme for CZ-accelerated sulfur vulcanization of unfilled NR.

3.4. Discussion on the mechanism of accelerating effect of graphene

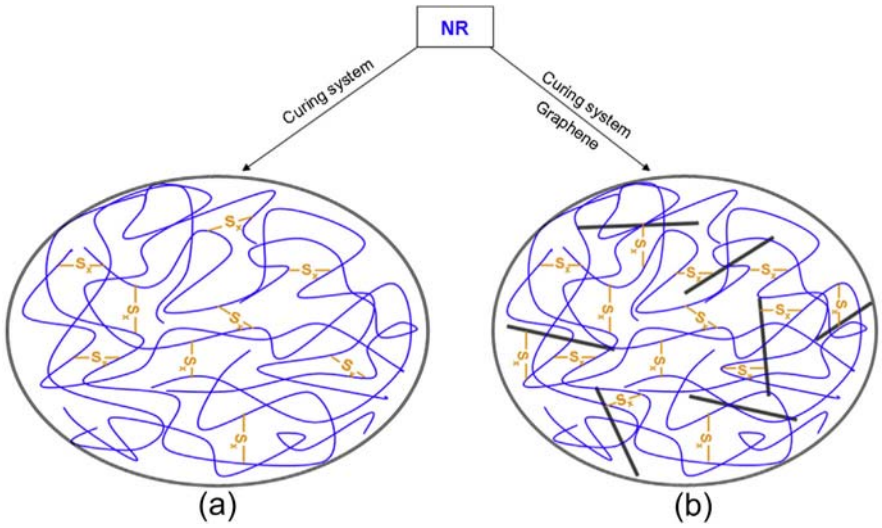
To further demonstrate the accelerating effect of graphene, we performed DSC measurement directly on the curing systems with or without graphene. It is shown in Fig. 13 that the melting peak of sulfur in the curing system, including sulfur, CZ, ZnO and SA with a weight ratio of 2:0.9:5:1, appears at 97.8 °C, while with the addition of graphene (1/2 the weight of sulfur) the melting peak is depressed to 90.4 °C. Only after melting, could the sulfur molecules diffuse to form polysulfide species and crosslinking points. Thus the lower melting peak in the curing system with graphene probably leads to lower curing temperature or shorter induction period.

Anther phenomenon should be noted in Fig. 13 is that the curing system without graphene shows an exothermal peak at 163.8 °C, incorporation of graphene significantly depresses the peak to 123.5 °C. Because there are no rubber molecules in the system, the exothermal peak can be attributed to the formation of polysulfide species. Therefore, the presence of graphene greatly accelerates the reactions between activator, accelerator and sulfur. The general reactions taking place in the N-cyclohexylbenzothiazole-2-sulfenamide accelerated formula are shown in Scheme 1 [1,40,41]. At first, the accelerator molecules react with themselves to give disulfide compounds, which then further react with sulfur to generate monomeric polysulfides with the structure of Bt–S–S_x–S–Bt, where



Scheme 2. Reaction scheme for CZ-accelerated sulfur vulcanization of GE/NR nanocomposites.

Author's personal copy



Scheme 3. Schematic representation of the network structures of unfilled NR (a) and GE/NR nanocomposites (b).

Bt is an organic radical derived from the accelerator (benzothiazyl). The monomeric polysulfides interact with the unsaturated sites on the rubber chains to form crosslink precursors, which are accelerator-terminated polysulfidic pendant groups attached to the rubber chains, such as rubber–Sx–S–Bt (sulfurated rubber). Finally, the crosslink precursors react, either directly with additional unsaturated sites or with other crosslink precursors, to give polysulfidic crosslinks (rubber–Sx–rubber) [1,40,41]. We consider that the addition of graphene may bring about additional reactions, in addition to the processes mentioned above. It was reported that the hydroxyl (–OH) and carboxyl (–COOH) groups on the carbon nanotubes could be converted into thiol (–SH), thioester (–CSOR), and dithiocarboxylic ester (–CSSR) groups upon reaction with sulfur [47,48]. Theoretical calculation also suggests that carbon nanotubes and graphene can be doped with sulfur [49,50]. Accordingly, we propose that graphene even after reduction bears –OH and –COOH groups, which could also undergo the same reaction to give –SH, –CSOR and –CSSR groups. The –SH, –CSOR and –CSSR groups interact with accelerator and sulfur, thus polysulfides species are generated to attack the unsaturated sites and form crosslinks. Scheme 2 presents one possible reaction route.

To sum up, graphene depresses the melting point of sulfur on one hand, and plays as a role of accelerator on the other hand. Both these two factors result in lower curing temperature or shorter induction period of the vulcanization of NR. Because graphene takes part in the vulcanization process, the network structure of GE/NR nanocomposites is different from that of unfilled NR. As shown in Scheme 3, graphene provides additional crosslinks, leading to higher crosslinking density of the GE/NR nanocomposites, which is confirmed by the curemeter and swelling measurements.

4. Conclusions

GE/NR nanocomposites were prepared by a modified latex mixing method. The results suggest that the method is efficient in dispersing graphene in the NR matrix. Curemeter and DSC measurements indicate that the addition of a small amount of graphene greatly changes the vulcanization kinetics of NR. The induction period of the vulcanization process is drastically suppressed at low graphene loading and then shows a gentle decrease, at the same time the vulcanization rate is enhanced at first and subsequently shows a depression. The combination effect of these two aspects leads to a prominent reduction in optimum cure time at first and then a slight increase. Unfilled NR and GE/NR nanocomposites with graphene loading ≤ 0.3 phr display a single exothermal peak during the vulcanization process, which however is split into two peaks at higher graphene loading. We propose that the physical diffusion process of the curing agents may be the reason. Thus, the two peaks are attributed to two reaction stages, i.e., chemical reaction controlling stage and diffusion controlling stage. The chemical reaction controlling stage has lower activation energy than the diffusion controlling stage. Addition of graphene decreases the activation energy of the former stage, while has an opposite effect on the activation energy of the latter stage. Finally, we proposed a possible mechanism to interpret the accelerating effect of graphene on NR. The current work indicates that graphene can be used to tune the vulcanization kinetics of rubbers, in addition to the mechanical properties, gas permeability and electrical conductivity.

Acknowledgment

This work was financially supported by National Natural Science Foundation of China (grant No.: 51203096), the Ph.D. Programs Foundation of Ministry of Education of China (grant No. 20100181120020), Sichuan University and Natural Science Foundation of Shanxi Province (grant No.: 20100110015-2).

References

[1] Mark JE, Erman B, Eirich FR. Science and technology of rubber. 3rd ed. New York: Academic Press; 2005.
[2] Lopez-Manchado MA, Arroyo M, Herrero B, Biagiotti J. J Appl Polym Sci 2003;89:1–15.
[3] Lu YL, Ye FY, Mao LX, Li Y, Zhang LQ. Express Polym Lett 2011;5:777–87.
[4] Avalos F, Ortiz JC, Zitzumbo R, López-Manchado MA, Verdejo R, Arroyo M. Europ Polym J 2008;44:3108–15.
[5] Lopez-Manchado MA, Herrero B, Arroyo M. Polym Int 2003;52:1070–7.
[6] Sun Y, Luo Y, Jia D. J Appl Polym Sci 2008;107:2786–92.
[7] Kader MA, Nah C. Polymer 2004;45:2237–47.
[8] Lakshminarayanan S, Gelves GA, Sundararaj U. J Appl Polym Sci 2012;124:5056–63.
[9] Sepehri A, Razzaghi-Kashani M, Ghoreishy MHR. J Appl Polym Sci 2012;125:E204–13.
[10] Lopez-Manchado MA, Biagiotti J, Valentini L, Kenny JM. J Appl Polym Sci 2004;92:3394–400.
[11] Sui G, Zhong W, Yang X, Zhao S. Macromol Mater Eng 2007;292:1020–6.
[12] Shanmugharaj A, Bae J, Lee K, Noh W, Lee S, Ryu S. Compos Sci Technol 2007;67:1813–22.

Author's personal copy

[13] Falco AD, Marzocca AJ, Corcuera MA, Eceiza A, Mondragon I, Rubiolo GH, et al. J Appl Polym Sci 2009;113:2851–7.
[14] Du M, Guo B, Lei Y, Liu M, Jia D. Polymer 2008;49:4871–6.
[15] Nie YJ, Huang GS, Qu LL, Zhang P, Weng GS, Wu JR. J Appl Polym Sci 2010;115:99–106.
[16] Akhlaghi S, Kalaee M, Mazinani S, Jowdar E, Nouri A, Sharif A, et al. Thermochimica Acta 2012;527:91–8.
[17] Stankovich S, Dikin DA, Dommett GHB, Kohlhaas KM, Zimney EJ, Stach EA, et al. Nature 2006;442:282–6.
[18] Ramanathan T, Abdala AA, Stankovich S, Dikin DA, Herrera-Alonso M, Piner RD, et al. Nat Nanotechnol 2008;3:327–31.
[19] Kim H, Miura Y, Macosko CW. Chem Mater 2010;22:3441–50.
[20] Kim H, Abdala AA, Macosko CW. Macromolecules 2010;43(16):6515–30.
[21] Kuilla T, Bhadra S, Yao D, Kim NH, Bose S, Lee JH. Prog Polym Sci 2010;35:1350–75.
[22] Young RJ, Kinloch IA, Gong L, Novoselov KS. Compos Sci Technol 2012;72:1459–76.
[23] Prud'Homme RK, Ozbas B, Aksay I, Register R, Adamson D. Functional graphene rubber nanocomposites. In: Patent US, editor. United States Patent, vol. US7745528B2. US: The Trustees of Princeton University; 2010. p. 1–80.
[24] Zhan Y, Lavorgna M, Buonocore G, Xia H. J Mater Chem 2012;22:10464–8.
[25] Zhan YH, Wu JK, Xia HS, Yan N, Fei GX. Macromol Mater Eng 2011;296:590–602.
[26] Potts JR, Shankar O, Du L, Ruoff RS. Macromolecules 2012;45:6045–55.
[27] Kim JS, Hong S, Park DW, Shim SE. Macromol Res 2010;18:558–65.
[28] Wu JR, Huang GS, Li H, Wu SD, Liu YF, Zheng J. Polymer 2013;54:1930–7.
[29] Hernández M, Bernal MDM, Verdejo R, Ezquerra TA, López-Manchado MA. Compos Sci Techol 2012;73:40–6.
[30] Bai X, Wan C, Zhang Y, Zhai Y. Carbon 2011;49:1608–13.
[31] Tang Z, Kang H, Shen Z, Guo B, Zhang L, Jia D. Macromolecules 2012;45:3444–51.
[32] Hummers WS, Offeman RE. J Am Chem Soc 1958;80:1339.
[33] Weng GS, Huang GS, Qu LL, Nie YJ, Wu JR. J Phys Chem B 2010;114:7179–88.
[34] Sahoo S, Maiti M, Ganguly A, Jacob George J, Bhowmick AK. J Appl Polym Sci 2007;105:2407–15.
[35] Stankovich S, Dikin DA, Piner RD, Kohlhaas KA, Kleinhammes A, Jia Y, et al. Carbon 2007;45:1558–65.
[36] Yang D, Velamakanni A, Bozoklu G, Park S, Stoller M, Piner RD, et al. Carbon 2009;47:145–52.
[37] Zhao X, Zhang Q, Chen D, Lu P. Macromolecules 2010;43:2357–63.
[38] Fan Z-J, Kai a, Yan J, Wei T, Zhi L-J, Feng J, et al. ACS Nano 2011;5:191–8.
[39] Paredes JI, Villar-Rodil S, Solis-Fernandez P, Martinez-Alonso A, Tascon JMD. Langmuir 2009;25:5957–68.
[40] Ghosh P, Katare S, Patkar P, Caruthers JM, Venkatasubramanian V. Rubber Chem Technol 2003;76:592–693.
[41] Coran AY. J Appl Polym Sci 2003;87:24–30.
[42] Flory PJ. Principles of polymer chemistry. Ithaca, NY: Cornell University Press; 1953.
[43] Arroyo M, López-Manchado MA, Herrero B. Polymer 2003;44:2447–53.
[44] Ding R, Leonov AI, Coran AY. Rubber Chem Technol 1996;69:81–91.
[45] Ozawa T. Bull Chem Soc Jpn 1965;38:1881–6.
[46] Kissinger HE. Anal Chem 1957;29:1702–6.
[47] Čech J, Curran SA, Zhang D, Dewald JL, Avadhanula A, Kandadai M, et al. Phys Status Solidi (b) 2006;243:3221–5.
[48] Curran SA, Cech J, Zhang D, Dewald JL, Avadhanula A, Kandadai M, et al. J Mater Res 2011;21:1012–8.
[49] Denis PA, Faccio R. Chem Phys Lett 2008;460:486–91.
[50] Denis PA, Faccio R, Mombru AW. ChemPhysChem 2009;10:715–22.
[51] Li H, Wu SD, Wu JR, Huang GS. Colloid Polym Sci. doi:10.1007/s00396-013-2959-0.
[52] Wang JD, Zhu YF, Zhou XW, Sui G, Liang J. J Appl Polym Sci 2006;100:4697–702.
[53] Bhowmick AK, De SK. Rubber Chem Technol 1979;52:985–95.